Molecular Therapy
Original Article

Apoptotic vesicles activate autophagy in recipient cells to induce angiogenesis and dental pulp regeneration

Zihan Li,[1,2,6] Meiling Wu,[1,6] Siying Liu,[2,6] Xuemei Liu,[1,2] Yu Huan,[3] Qingyuan Ye,[2,4] Xiaoxue Yang,[1] Hao Guo,[1] Anqi Liu,[1] Xiaoyao Huang,[1] Xiaoshan Yang,[2,5] Feng Ding,[2] Haokun Xu,[2] Jun Zhou,[2] Peisheng Liu,[1] Shiyu Liu,[2] Yan Jin,[2] and Kun Xuan[1]

[1]State Key Laboratory of Military Stomatology and National Clinical Research Center for Oral Diseases and Shaanxi Clinical Research Center for Oral Diseases, Department of Preventive Dentistry, School of Stomatology, The Fourth Military Medical University, 145West Changle Road, Xi'an, Shaanxi, China; [2]State Key Laboratory of Military Stomatology and National Clinical Research Center for Oral Diseases and Shaanxi International Joint Research Center for Oral Diseases, Center for Tissue Engineering, School of Stomatology, The Fourth Military Medical University, 145West Changle Road, Xi'an, Shaanxi, China; [3]Department of Neurosurgery, Xijing Hospital, Air Force Medical University, Xi'an, Shaanxi, China; [4]State Key Laboratory of Military Stomatology and National Clinical Research Center for Oral Diseases and Shaanxi Engineering Research Center for Dental Materials and Advanced Manufacture, Department of Periodontology, School of Stomatology, The Fourth Military Medical University, Xi'an, Shaanxi, China; [5]Stomatology Hospital, Southern Medical University, Guangzhou, Guangdong, China

Extracellular vesicles (EVs) derived from living cells play important roles in donor cell-induced recipient tissue regeneration. Although numerous studies have found that cells undergo apoptosis after implantation in an ischemic-hypoxic environment, the roles played by the EVs released by apoptotic cells are largely unknown. In this study, we obtained apoptotic vesicles (apoVs) derived from human deciduous pulp stem cells and explored their effects on the dental pulp regeneration process. Our work showed that apoVs were ingested by endothelial cells (ECs) and elevated the expression of angiogenesis-related genes, leading to pulp revascularization and tissue regeneration. Furthermore, we found that, at the molecular level, apoV-carried mitochondrial Tu translation elongation factor was transported and regulated the angiogenic activation of ECs via the transcription factor EB-autophagy pathway. In a beagle model of dental pulp regeneration *in situ*, apoVs recruited endogenous ECs and facilitated the formation of dental-pulp-like tissue rich in blood vessels. These findings revealed the significance of apoptosis in tissue regeneration and demonstrated the potential of using apoVs to promote angiogenesis in clinical applications.

INTRODUCTION

A well-functioning blood vascular system is essential to tissue regeneration, and in transplantation, it participates in gas exchange, nutrient transport, and waste clearance between the donor and host tissues.[1] However, endogenous endothelial cells (ECs) seldom proliferate, remaining in an inactive state for decades in adult life,[2,3] which results in slow and inefficient revascularization, and ultimately, tissues fail to regenerate,[4] especially ischemic-hypoxic tissues.[5] Thus, revascularization of ischemic-hypoxic tissue remains an unmet medical need despite the remarkable effectiveness of regenerative medicine of a variety of tissues.

Mesenchymal stem cell (MSC) transplantation has been confirmed to have beneficial effects by activating the angiogenic function of host ECs and achieving regeneration efficiency in ischemic tissues.[6] Recent reports have shown that the ischemic-hypoxic environment activates the angiogenic potential of MSCs, including their ability to release angiogenic factors,[7] secrete exosomes,[8] and alter EC behavior.[9] However, the ischemic-hypoxic environment usually leads to the apoptosis of the donor cells,[10] which is not conducive to favorable revascularization or effective regeneration. Moreover, whether apoptosis influences angiogenesis is largely unclear, and the potential mechanisms are unknown.

Apoptosis is an autonomously regulated cellular end-of-life process and is considered to be a passive phenomenon.[11] This view is beginning to change, as studies have shown that apoptosis plays an important role in regulating tissue homeostasis and promoting tissue

Received 14 December 2021; accepted 7 May 2022;
https://doi.org/10.1016/j.ymthe.2022.05.006.

[6]These authors contributed equally

Correspondence: Shiyu Liu, PhD, Research and Development Center for Tissue Engineering, School of Stomatology, The Fourth Military Medical University, 145West Changle Road, Xi'an, Shaanxi 710032, China.
E-mail: liushiyu@vip.163.com
Correspondence: Yan Jin, PhD, Research and Development Center for Tissue Engineering, School of Stomatology, The Fourth Military Medical University, 145West Changle Road, Xi'an, Shaanxi 710032, China.
E-mail: yanjin@fmmu.edu.cn
Correspondence: Kun Xuan, PhD, Department of Preventive Dentistry, School of Stomatology, The Fourth Military Medical University, 145West Changle Road, Xi'an, Shaanxi 710032, China.
E-mail: xuankun@fmmu.edu.cn

repair and regeneration.[12,13] Apoptotic cells can release a variety of substances that regulate body homeostasis, including metabolites and extracellular vesicles (EVs). It has been reported that these specific metabolites can act as good-bye signals to actively modulate the biological functions of neighboring cells.[14,15] Moreover, apoptotic vesicles (apoVs), types of EVs, can also transfer multifarious substances, including microRNAs (miRNAs), proteins, and lipids, that initiate signal transduction.[16] EVs have been reported to promote angiogenesis during the regeneration process.[17] However, the mechanisms through which apoVs influence angiogenesis and tissue regeneration remain unclear.

In recent years, MSC transplantation has led to significant outcomes in the field of maxillofacial regeneration.[18,19] We previously showed that aggregated human deciduous pulp stem cell (hDPSC) transplantation enabled the morphological and functional regeneration of full-length dental pulp, but the underlying mechanism remains unclear.[20] Dental pulp is a vascular-rich tissue in the stable root canal, which is connected to surrounding tissue only through the apical foramen;[21] this special structure provides a powerful model to discover the significance of apoptosis and explore the function of apoVs in vascularization and tissue regeneration. Moreover, translational application of apoVs may help establish a potential noncellular treatment for tissue regeneration in an ischemic-hypoxic environment.

In this study, we first explored the effect of hDPSC apoptosis on dental pulp regeneration. Then, we prepared apoptotic vesicles derived from hDPSCs (hDPSC-apoVs) and tested their proangiogenic effect on ECs. Then, we tested the ability of apoVs to stimulate angiogenesis and improve blood supply to the root canal. Mechanistically, we demonstrated that hDPSC-apoVs promoted EC autophagy by transferring mitochondrial Tu translation elongation factor (TUFM). Furthermore, autophagy signaling activated the angiogenic potential of ECs. Taken together, our findings indicated that apoVs can activate autophagy of recipient cells to induce host blood vessels to grow in ischemic-hypoxic environments, providing additional insights into improvements for tissue regeneration.

RESULTS

Aggregated hDPSCs undergo apoptosis that leads to dental pulp regeneration

Dental pulp is crucial for maintaining tooth vitality. However, its limited self-repair capacity makes dental pulp vulnerable to necrosis by trauma and infections.[22] In addition, the restriction of blood supply through the narrow apical foramen makes regeneration particularly difficult, which leads to the apoptosis of donor cells.[23] We investigated this outcome using an athymic nude mouse model (the details are presented in the materials and methods section).

First, we characterized the hDPSCs used in this study. Flow cytometry results showed that hDPSCs highly expressed CD105, CD73, and CD90 but not CD45, CD34, CD14, CD19, and HAL-DR (Figure S1A). Alizarin red staining and oil red O (ORO) staining indicated that these cells exhibited osteogenic and lipogenic differentiation potential (Figure S1B). Crystalline violet staining showed that hDPSCs generated single colony clusters (Figure S1C).

Then, we prepared human tooth scaffolds combined with aggregated hDPSCs (the hDPSC group) or PBS gel (the control [Ctrl] group) and implanted them into the dorsum of athymic nude mice (Figures 1A and 1B). After 2 months, hematoxylin-eosin (H&E) staining showed the formation of dental-pulp-like tissue in the hDPSC group (Figure 1C). To verify the H&E histology, we performed immunofluorescence staining, which also showed the presence of dentin sialophosphoprotein (DSPP)- and dentin matrix protein 1 (DMP1)-positive odontoblast layers in newly formed tissue, which was similar to the natural dental pulp structure (Figure 1D).

To elucidate whether these cells undergo apoptosis, aggregated hDPSCs were implanted in an ischemic-hypoxic environment. TUNEL staining results showed that a significant portion of the aggregated hDPSCs underwent apoptosis 24, 48, or 72 h after implantation (Figure 1E). We also validated this result using flow cytometry and found that the ratio of apoptotic cells among the aggregated cells reached 47% within 72 h (Figure 1F). These data demonstrate that aggregated hDPSCs underwent apoptosis shortly after implantation.

Apoptosis of aggregated hDPSCs was necessary for dental pulp regeneration

To explore the role played by apoptosis in dental pulp regeneration, we pretreated aggregated hDPSCs with Z-VAD, an apoptosis inhibitor, and the inhibition efficiency was verified by TUNEL staining (Figure S2D). We implanted tooth scaffolds filled with aggregated hDPSCs (the hDPSC group) or aggregated hDPSC pretreated with Z-VAD (the Z-VAD group) subcutaneously in the dorsum of athymic nude mice. After 2 months, H&E staining results showed that the mice in the hDPSC group formed good dental-pulp-like tissues, as expected (Figure 2A). In contrast, the Z-VAD group mice failed to achieve dental pulp regeneration after apoptosis inhibition. In addition, the donor cells underwent necrosis due to insufficient blood supply (Figure 2B). These results suggest that apoptosis was necessary for aggregated hDPSC-induced dental pulp regeneration.

Stem cells can release an abundance of EVs that contain functional elements that are useful for tissue regeneration.[17] The role played by apoVs released by apoptotic cells during dental pulp regeneration deserves further investigation. We induced hDPSC apoptosis with STS, a protein kinase C inhibitor (Figure S1D). Next, we isolated apoVs from apoptotic hDPSCs using a gradient centrifugation protocol (Figure S2A) and characterized apoV morphology (Figures 2C, 2D, and S2C). The size distribution of the apoVs was tested by dynamic light scattering (Figure 2E). Then, fluorescence staining and flow cytometry were performed to detect the exposure of phosphatidylserine (PtdSer), a specific marker of apoVs (Figures 2F and S2B). A western blot analysis showed that apoVs expressed a high level of cleaved caspase-3 (Figure 2G). These results indicated the effective extraction of apoVs.

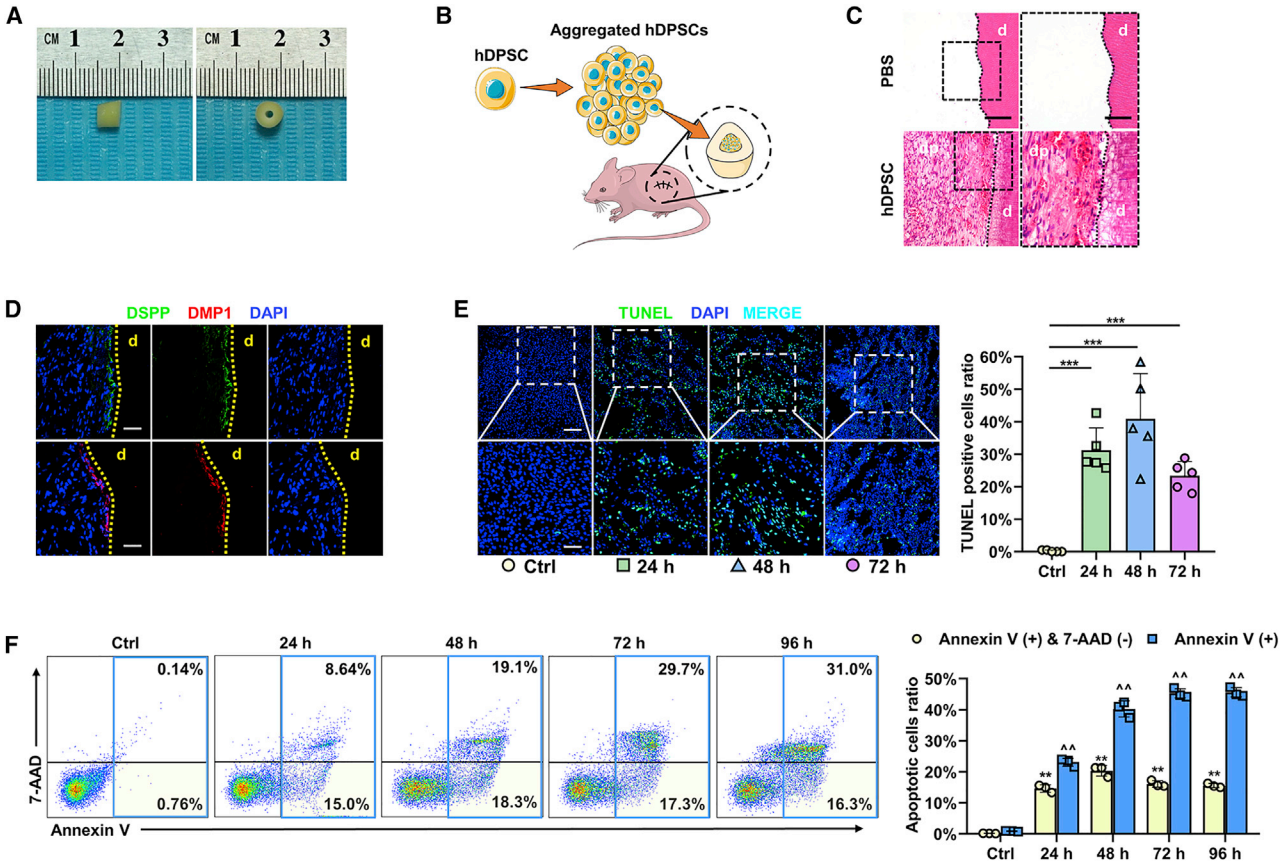

Figure 1. Aggregated hDPSCs undergo apoptosis shortly after implantation

(A) Preparation of implanted tooth scaffold, with a height of 5 mm. (B) Schematic of the tooth transplantation process in the dorsum of athymic nude mice. Tooth scaffolds were filled with aggregated hDPSC. (C) H&E staining shows the regeneration of dental-pulp-like tissue; dp, dental pulp; d, dentin. Scale bars, 100 μm in low-magnification images and 50 μm in high-magnification images. (D) Immunofluorescence analysis shows the expression of odontogenic differentiation markers DSPP and DMP1, with positive staining represented by green and red stains. DSPP, dentin sialophosphoprotein; DMP1, dentin matrix protein 1; d, dentin. Scale bars, 100 μm. (E) TUNEL staining shows the apoptosis ratio of aggregated hDPSCs before transplantation (Ctrl), or 24, 48, or 72 h after transplantation. Scale bars, 100 μm in low-magnification images and 50 μm in high-magnification images; n = 5 per group. (F) Flow cytometry analysis shows the apoptosis ratio of aggregated hDPSC before transplantation (Ctrl), or 24, 48, 72, or 96 h after transplantation. *Annexin V (+) and 7-AAD (–) cell ratio compared with Ctrl; ^annexin V (+) cells ratio compared with Ctrl; n = 3 per group. Data are presented as mean ± SD. Statistical analyses were performed by one-way ANOVA with Tukey's post hoc test or Welch's ANOVA with Games-Howell post hoc test. *p < 0.05, **/^^p < 0.01, ***p < 0.001; ns, p > 0.05.

Then, we inserted aggregated hDPSCs pretreated with Z-VAD (the Z-VAD group), aggregated hDPSCs supplemented with hDPSC-apoVs (the hDPSC + apoV group), and Z-VAD-pretreated aggregated hDPSCs supplemented with hDPSC-apoVs (the Z-VAD + apoV group) into the tooth scaffolds. Two months after *in vivo* implantation in the dorsum of athymic nude mice, H&E staining showed a reduced necrotic area and angiogenesis near the opening of the tooth scaffolds in the Z-VAD + apoV group compared with those in the Z-VAD group (Figures 2H, 2I, and 2K. Compared with the effect on the hDPSC group, supplementation with apoVs induced angiogenesis in the newly formed dental-pulp-like tissue (Figures 2A and 2J). We then labeled CD31 in blood vessels. Confocal microscopy images showed increased vascular density in the groups treated with apoVs (Figure 2K). Collectively, these results provide strong evidence indicating that hDPSC apoptosis plays an active role in dental pulp regeneration and that apoVs can promote the formation of blood vessels.

hDPSC-apoVs promote tissue regeneration

We further explored whether apoVs individually promote blood vessel regeneration in the root-canal space. Scaffolds filled with PBS gel (the PBS group) or hDPSC-apoVs gel (the apoV group) were implanted into the dorsum of athymic nude mice. After 2 months, H&E staining showed the formation of dental-pulp-like tissue in the apoV group relative to the loosely aligned connective tissue in the PBS group (Figures 3A and 3B [i and ii]). Additionally, a significant increase in de novo dentin-like tissue was found in the apoV group through H&E and Masson's staining (demarcated by dashed yellow lines in Figures 3A and 3B [iii and iv]). Concomitantly, higher vessel density was found in the apoV group

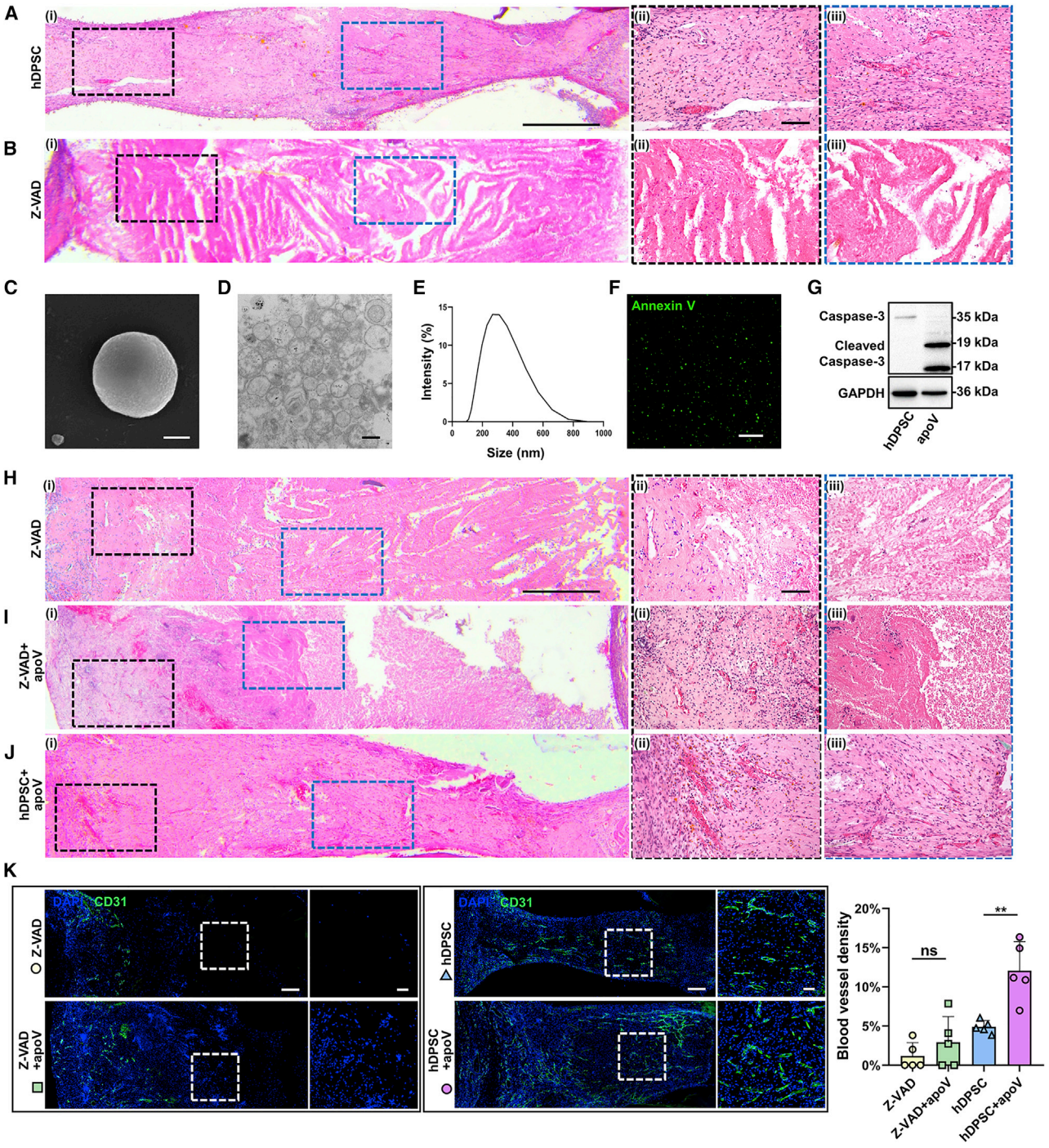

Figure 2. Apoptosis of hDPSCs after implantation promote the regeneration of dental pulp

(Ai and Bi) Representative microscope images of H&E staining show regeneration of dental pulp in tooth scaffolds. Scale bars, 0.5 mm. (Aii and iii and Bii and iii) Enlarged view of boxed area in (i). Scale bars, 100 μm. (A) Regularly prepared aggregated hDPSCs. (B) Aggregated hDPSCs pretreated with Z-VAD. (C–G) Characterization of hDPSC-apoVs. (C) Representative SEM image of apoVs. Scale bar, 200 nm. (D) Representative TEM image of apoVs. Scale bar, 500 nm. (E) Size distribution of apoVs. (F) Annexin V staining of apoVs. Scale bars, 200 μm. (G) Protein characterization of apoVs. (Hi–Ji) Representative microscope images of H&E staining show regeneration of dental pulp in Z-VAD group, Z-VAD + apoV group, and hDPSC + apoV. Scale bars, 0.5 mm. (Hii and iii–Jii and iii) Enlarged view of boxed area in (i). Scale bars, 100 μm. (H) Aggregated

(legend continued on next page)

(Figures 3A and 3B [v]), which suggested that apoVs promoted blood vessel regeneration *in vivo*.

Considering the favorable angiogenesis outcome induced by apoVs, we further investigated the angiogenic effects of apoVs and compared the effects with the degree of dental pulp revascularization, which is a novel clinical therapy. We constructed a preclinical large-animal (dog) model (the details are presented in Materials and methods), and dental pulp in the incisors (a total of 36 teeth in 6 dogs) was extracted with a mechanical method. The revascularization treatment (the Revas group) or apoV gel treatment (the apoV group) was performed on the incisors, and the results were compared with those obtained with a PBS gel (the PBS group), which was the control. Three months after treatment, H&E staining showed that no fibrous connective tissue had formed in the PBS group (Figure 3D [i]), which verified dental pulp ablation.

Cone-beam computed tomography (CBCT) images of the incisors were taken, and 3D images were reconstructed before and 3 months after treatment. Compared with that in the PBS group, the dentin thickness increased by an average of 0.2 cm in the apoV group, but the increase in the Revas groups was not statistically significant (Figure 3C), which demonstrated that apoVs promoted the development of young permanent teeth.

Dental-pulp-like tissue contained newly formed blood vessels in the apoV group (Figure 3F), but after the revascularization treatment, only the formation of some amorphous matrixes was observed (Figure 3E). Immunofluorescence staining ultimately showed CD31-positive cells arranged in lumen-like shapes in the apoV group (Figure 3G). Together, these results demonstrated that hDPSC-apoVs promoted dental pulp regeneration by stimulating angiogenesis.

hDPSC-apoVs are internalized by ECs and enhance their angiogenic capacities

To investigate how hDPSC-apoVs promote angiogenesis, we labeled apoVs with PKH26 and cocultured them with human umbilical vein ECs for 8 h. Confocal microscopy images showed that the apoVs localized within ECs (Figure 4A). A western blot analysis showed that the expression of angiogenesis- and cell migration-associated proteins (HIF-1α, VEGF, ANG2, and MMP2) in ECs were significantly upregulated after treatment (Figure 4B). We next investigated the effect of apoVs on EC functions.

A Matrigel assay showed that 20 μg/mL apoVs significantly promoted EC tube formation, and the tube formation ability of these cells persisted for a long time (Figures 4C–4E). Furthermore, a Transwell assay showed that the number of migrated ECs was increased after apoVs treatment in a concentration-dependent manner (Figure 4F). In addition, we assessed the effect of apoVs on EC proliferation by performing a MKI67/Ki67 assay, and the results showed that the percentage of Ki67-positive cells significantly increased after apoV treatment, indicating that apoVs promoted EC proliferation (Figure 4G). Thus, these data indicated that the internalization of hDPSC-apoVs directly enhanced the angiogenic capacity of the ECs *in vitro*.

hDPSC-apoVs regulate EC function by inducing autophagy

EVs regulate receptor cell function via the transfer of proteins, lipids, and nucleic acids.[24] Therefore, we identified the proteomic compositions of hDPSCs and apoVs by using mass spectrometry. A total of 9,424 proteins were identified in hDPSCs and apoVs. Among the 1,102 differentially expressed proteins between the hDPSCs and apoVs, 129 were significantly upregulated in the apoVs (Figures S3A and S3B). We then focused on the pathway enriched with the upregulated proteins by performing a Kyoto Encyclopedia of Genes and Genomes (KEGG) pathway analysis; the results showed that the proteins were enriched in autophagy-associated pathways, such as the "mTOR-signaling pathway," "mitophagy-animal," and "insulin-signaling pathway" (Figure S3E). These results indicated that hDPSC-apoVs contained many proteins that were highly related to autophagy, which might exhibit regulatory functions in ECs.

Therefore, we detected the autophagy level in ECs after apoV treatment. Western blot results showed that the expression of autophagy-associated proteins (ATG7, Beclin-1, and LC3) were upregulated (Figure 5A). In addition, we infected ECs with adenoviruses expressing mRFP-GFP-LC3 to inhibit the change in autophagic flux in the intracellular space. Confocal microscopy images showed the formation of autophagosomes (both mRFP and GFP fluorescence emitted a yellow signal) and autolysosomes (only red RFP fluorescence was emitted) after apoV treatment. By blocking the fusion of autophagosomes with lysosomes by treating cells with chloroquine (CQ), we observed the accumulation of autophagosomes in the apoV group over time (Figure 5B). Similarly, a western blot analysis also showed increased expression of LC3 II (microtubule-associated protein 1 light-chain 3 II) 4, 12, or 24 h after treatment of ECs with CQ (Figure 5C). Taken together, these data demonstrate that apoVs activate EC autophagy.

Autophagy is known to regulate homeostasis during angiogenesis and to increase the vascular system.[25] To determine whether autophagy performs a similar function in apoV-mediated angiogenesis, we treated ECs with 3-methyladenine (3-MA), an autophagy inhibitor, and observed the change in EC angiogenic activities after apoV treatment. As expected, the angiogenic, migratory, and proliferative functions of the ECs were reduced after autophagy inhibition

hDPSCs pretreated with Z-VAD. (I) Aggregated hDPSCs pretreated with Z-VAD supplemented with apoVs. (J) Regularly prepared aggregated hDPSCs supplemented with apoVs. (K) Immunofluorescence analysis shows the vessel density of regenerated dental pulp tissue. Scale bars, 200 μm in low-magnification images and 50 μm in high-magnification images; n = 5 per group. Data are presented as mean ± SD. Statistical analyses are performed by one-way ANOVA with Tukey's post hoc test or Welch's ANOVA with Games-Howell post hoc test. *$p < 0.05$, **$p < 0.01$, ***$p < 0.001$; ns, $p > 0.05$.

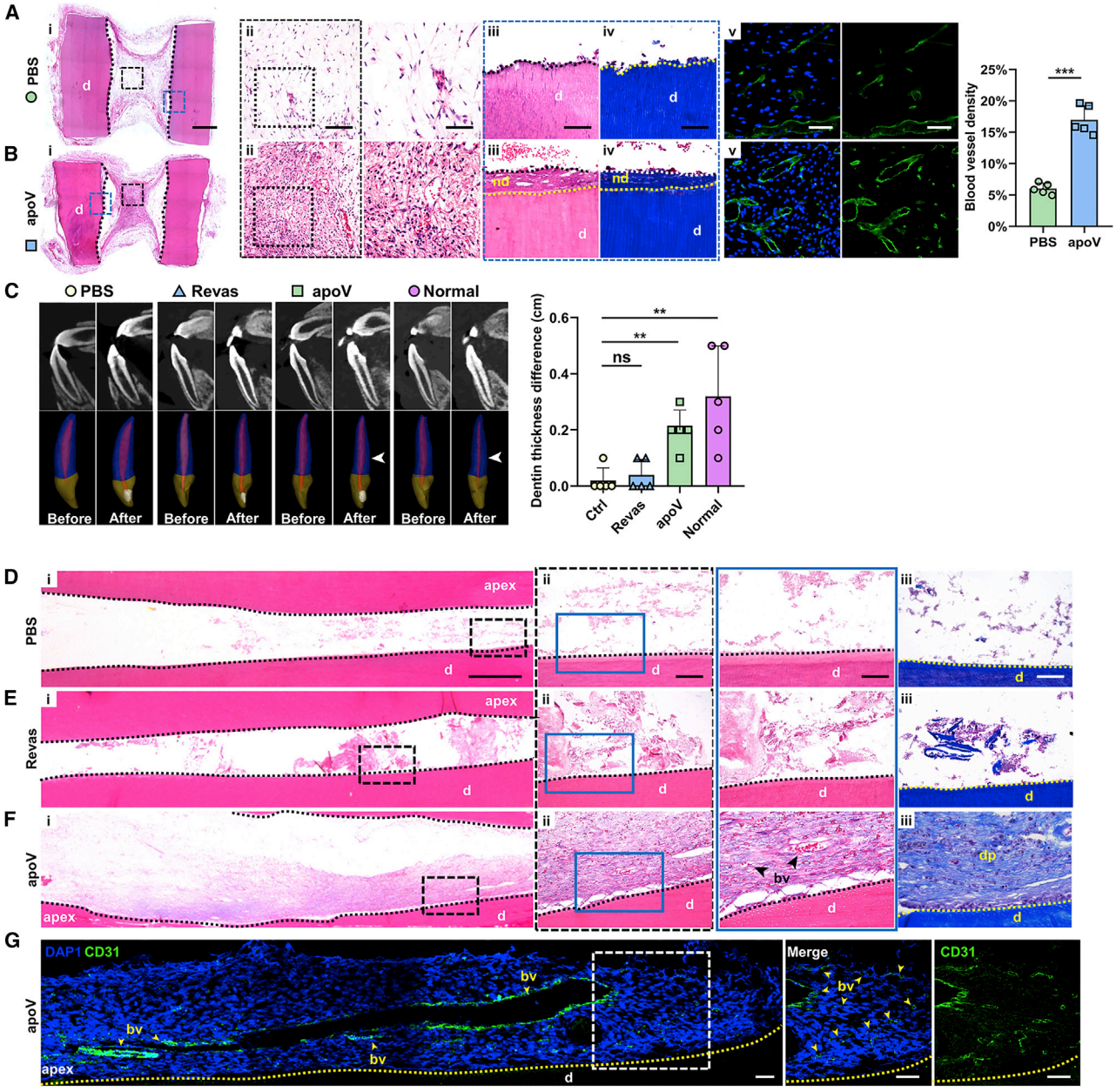

Figure 3. hDPSC-apoVs induce angiogenesis and dental pulp regeneration *in vivo*

(AI and Bi) Representative microscope images of H&E staining show regeneration of dental pulp in tooth scaffolds. Scale bars, 1 mm. (Aii and iii and Bii and iii) Enlarged view of boxed area in (i). Scale bars, 100 μm in low-magnification images and 50 μm in high-magnification images. (Aiv and Biv) Masson's Trichrome staining of boxed area in (i). (Av and Bv) Immunofluorescence analysis shows the vessel density in new-formation dental-pulp-like tissues. Scale bars, 100 μm in low-magnification images and 50 μm in high-magnification images; n=5 per group. (C) Representative CBCT images (top) of incisor teeth before and after treatment and 3D images (bottom) of incisor teeth before and after treatment. The amount of dentin was increased after treatment in the apoV and normal groups (white arrows); n = 5 per group. (Di and Fi) Representative microscope images of H&E staining show regeneration effect of dental pulp in beagle's incisor teeth. Scale bars, 0.5 mm. H&E and Masson's Trichrome staining of PBS group (Dii and iii), dental pulp revascularization (Revas) group (Eii and iii), and apoVs group (Fii and iii). Scale bars, 100 μm in low-magnification images and 50 μm in high-magnification images. (G) Immunofluorescence analysis shows the expression of blood vessel marker CD31, with positive represented by green stains. Scale bars, 200 μm in low-magnification images and 50 μm in high-magnification images. Apex, root tip of teeth; bv, blood vessels; dp, dental pulp; nd, newly formed dentin; d, dentin; n = 5 per group. Data are presented as mean ± SD. Statistical analyses were performed by Student's t test (two-tailed) for two group comparisons and one-way ANOVA with Tukey's post hoc test or Welch's ANOVA with Games-Howell post hoc test for multiple group comparisons. *p < 0.05, **p < 0.01, ***p < 0.001; ns, p > 0.05.

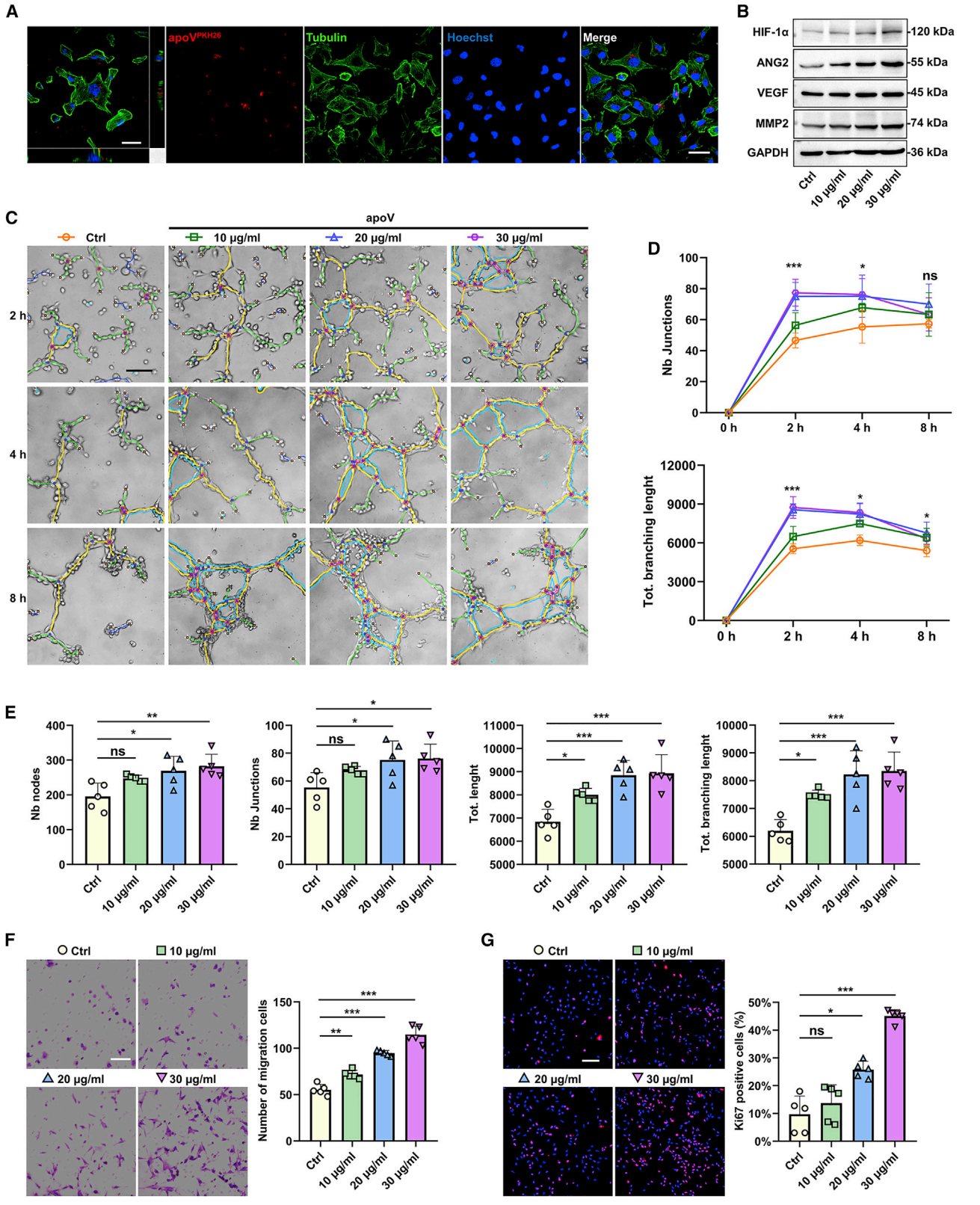

(legend on next page)

(Figures 5D–5G). All these results revealed that hDPSC-apoVs enhanced the EC angiogenic function via autophagy regulation.

TUFM activates EC autophagy via TFEB nuclear translocation

Notably, previous studies have elucidated that TUFM is an autophagy effector.[26] Therefore, we sought to determine whether TUFM derived from apoVs mediates autophagy in ECs. First, a western blot analysis was performed to verify the existence of TUFM in apoVs (Figure 6A). Then, we transfected hDPSCs with short interfering RNA (siRNA) against TUFM (si-*TUFM*) to downregulate the expression of TUFM in the apoVs (Figure 6A). Next, to determine the effects of TUFM on EC autophagy, we treated the ECs with two kinds of apoVs (apoVs and si-*TUFM*-apoVs), and unstimulated ECs comprised the control group. The results showed that the expression level of autophagy-associated genes was distinctly downregulated in the si-*TUFM*-apoV group (Figure 6B). Finally, we found that EC tube formation, migration, and proliferation were attenuated by downregulating the expression of TUFM in apoVs (Figures 6C–6E). These results indicated that TUFM derived from hDPSC-apoVs activated EC autophagy to regulate angiogenic capacity.

Several studies have confirmed that TUFM can regulate the TFEB-induced autophagy–lysosome pathway.[27] To investigate whether TUFM derived from hDPSC-apoVs activates EC autophagy in the same way that it induces TFEB-induced autophagy, we first labeled lysosomes to monitor lysosomal biogenesis. LysoTracker staining showed that the number of lysosomes was increased after apoV treatment, similar to the effect caused by Torin 1, a lysosomal activator (Figure 6F). Moreover, the expression of lysosomal-associated proteins (LAMP1 and CLCN7) and TFEB was upregulated (Figure 6G).

TFEB regulates the expression of autophagy-related genes by moving to the nucleus. We evaluated the content variations of TFEB in the nucleus after apoVs treatment. In the apoV group, TFEB expression in the nucleus was increased (Figure 6H), and TFEB nuclear translocation was observed by immunofluorescence (Figure 6I). Then, by increasing or decreasing TFEB expression levels in ECs, we confirmed that TFEB regulated autophagy. (Figures 6J and 6K). We further explored the effect of TFEB on EC angiogenic capacity. After TFEB knockdown, the tube formation, migration, and proliferation functions of the ECs induced by apoVs were attenuated (Figures 6L–6N). Collectively, these results revealed that TUFM derived from hDPSC-apoVs activated EC autophagy and promoted EC angiogenesis via the TFEB-induced autophagy-lysosome pathway.

hDPSC apoptosis ameliorates revascularization via autophagy *in vivo*

To verify that autophagy was necessary for apoV-mediated EC angiogenesis *in vivo*, we injected 3-MA into athymic nude mice to inhibit autophagy and then detected the expression of LC3 to determine the inhibition efficiency (Figure 7A). Then, we implanted tooth scaffolds filled with apoVs (the 3-MA + apoV group) subcutaneously in the dorsum of autophagy-inhibited athymic nude mice. H&E staining showed that apoVs did not induce the formation of blood vessels after autophagy inhibition (Figures 7B–7D). Thus, we considered that autophagy was required for apoV-mediated angiogenesis *in vivo*.

Taken together, our results led us to conclude that exogenous aggregated hDPSCs partially undergo apoptosis after implantation into the root canal. apoVs derived from hDPSCs specifically activated endogenous EC autophagy by transferring TUFM. Furthermore, autophagy signaling mediated EC biological behavior and caused angiogenesis. Eventually, the accelerated revascularization promoted the efficient regeneration of dental pulp. Significantly, the large-animal experiment verified the angiogenic function of the apoVs administered independently. Overall, these results identify an unreported mechanism of apoptosis in dental pulp regeneration (Figure 8).

DISCUSSION

As determined by their biogenesis, EVs can be divided into three main categories: exosomes, microvesicles, and apoVs. Formerly, the products of apoptotic cells were considered waste or deleterious substances.[11] Recently, mounting evidence has suggested that apoVs play key roles not only in the regulation of normal physiological processes, such as spermatogenesis,[28] renewal of the outer segment of photoreceptors,[29] and immune surveillance[30] but also in tissue repair and regeneration.[12,13] Our study confirmed that apoVs released by exogenous hDPSCs exerted positive effects on revascularization during stem-cell-mediated pulp regeneration and that apoV-loaded TUFM was transported to regulate the activation of endogenous ECs via the TFEB-induced autophagy pathway. Previous studies have shown that autophagy is a double-edged sword during angiogenesis and that the precise role played by autophagy in various organismic microenvironments might substantially differ. Our findings revealed that autophagy activated by hDPSC-apoVs promoted the angiogenic abilities of ECs, including their proliferation, migration, differentiation, and secretion. These findings facilitate our understanding of apoptosis in early tissue regeneration after stem cell transplantation and provide a reference for future studies.

Figure 4. hDPSC-apoVs enhance the angiogenic capacity of the ECs

(A) Representative confocal orthogonal view shows the uptake of PKH26-labeled apoVs (red) by ECs (green), counterstained with Hoechst (blue). Scale bar, 50 μm. (B) Western blot analysis shows the expressions of HIF-1α, VEGF, ANG2, and MMP2 in ECs after incubation with apoVs at concentrations of 10, 20, or 30 μg/mL for 12 h. (C–E) Matrigel analysis shows the effect of hDPSC-apoVs on tube formation capacity of ECs. Scale bar, 100 μm. (D) *Comparison between Ctrl and 20 μg/mL, (E) *compared with Ctrl. (F) Transwell assay shows the effect of hDPSC-apoVs on migration capacity of ECs. Scale bar, 100 μm. (G) Immunofluorescent staining of MKI67 shows the effect of hDPSC-apoVs on the proliferation capacity of ECs. Scale bar, 100 μm; n = 5 per group. Data are presented as mean ± SD. Statistical analyses were performed by Student's t test (two-tailed) or Student's t test with Welch correction (two-tailed) for two-group comparisons and one-way ANOVA with Tukey's post hoc test or Welch's ANOVA with Games-Howell post hoc test for multiple-group comparisons. *$p < 0.05$, **$p < 0.01$, ***$p < 0.001$; ns, $p > 0.05$.

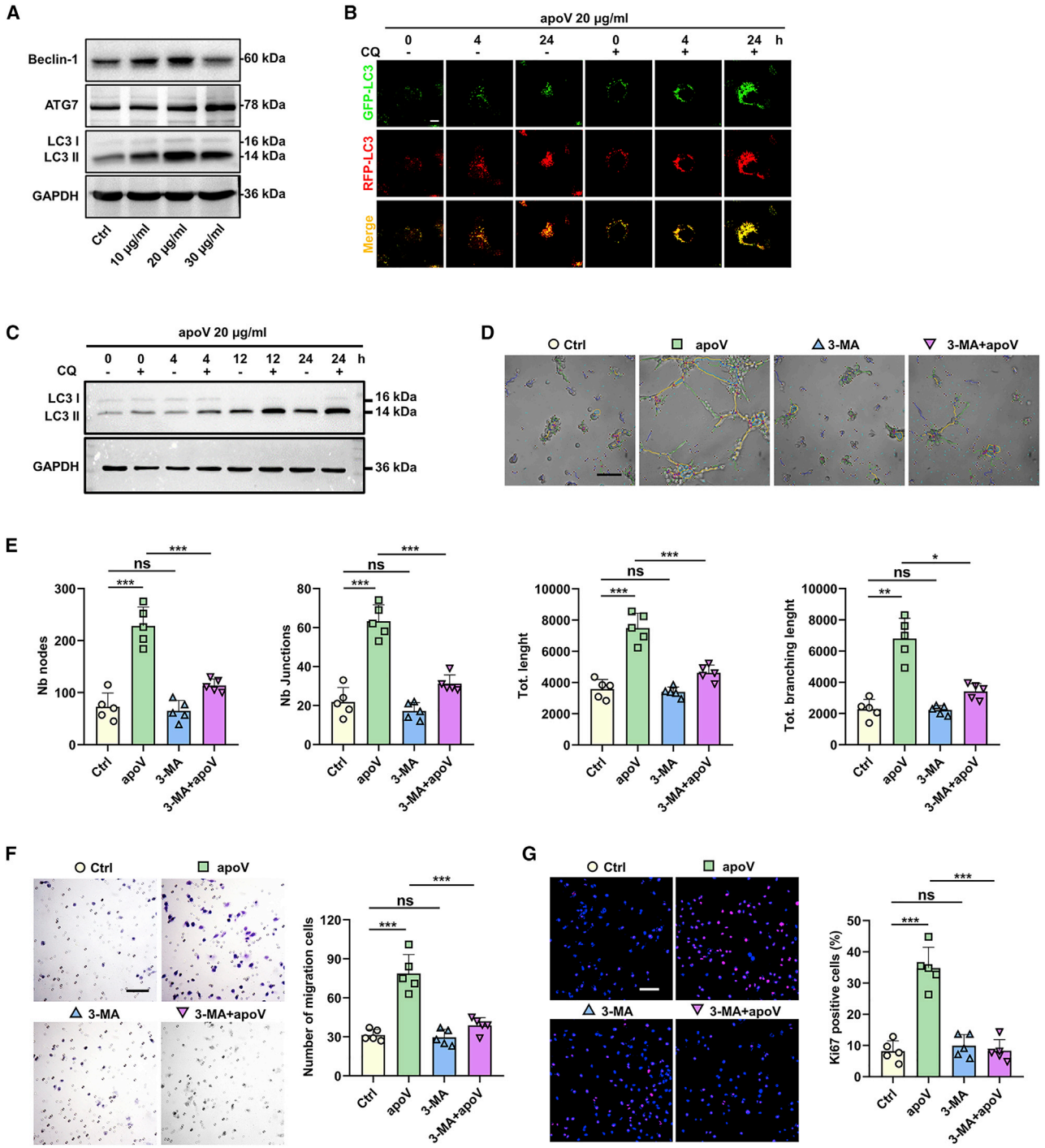

Figure 5. hDPSC-apoVs activate the autophagy of ECs to induce angiogenesis

(A) Western blot analysis shows autophagy-associated genes (ATG7, Beclin-1, and LC3) expression in ECs after incubation with apoVs at concentrations of 10, 20, or 30 μg/mL. (B) Representative confocal microscopy images show the numbers of autophagosomes (yellow) and autolysosomes (red) per cell. Scale bars, 10 μm. (C) Expression of LC3 in ECs cocultured with 20 μg/mL apoVs after treatment with or without CQ was evaluated by western blots at 0, 4, 12, or 24 h. After pretreatment with or without 3-MA, the angiogenic capacity of ECs, including tube formation (D and E), migration (F), and proliferation (G) were detected following coculture with apoVs (20 μg/mL). Scale bar, 100 μm; n = 5 per group. Data are presented as mean ± SD. Statistical analyses were performed by one-way ANOVA with Tukey's post hoc test or Welch's ANOVA with Games-Howell post hoc test for multiple-group comparisons. *$p < 0.05$, **$p < 0.01$, ***$p < 0.001$; ns, $p > 0.05$.

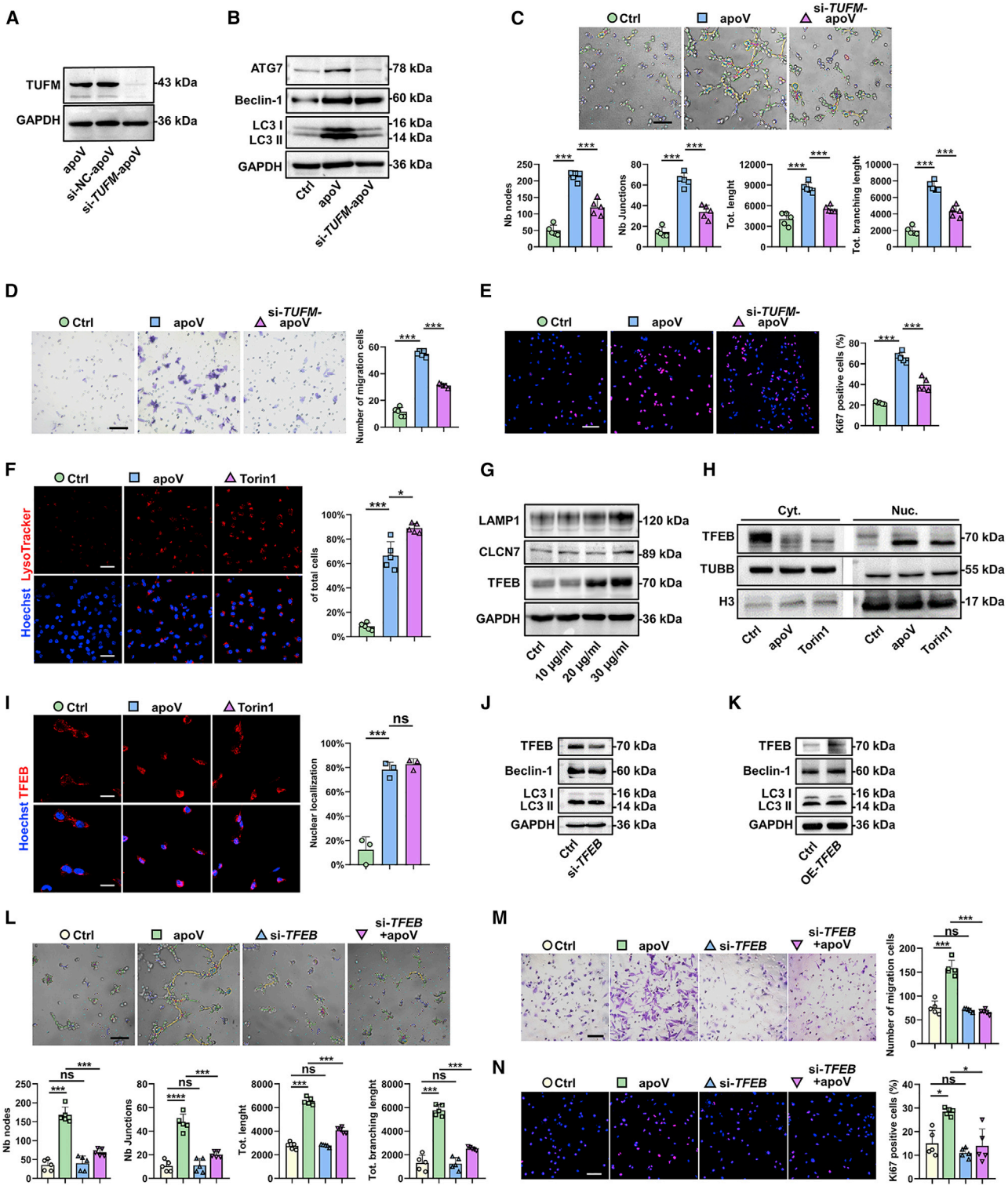

Figure 6. TUFM derived from hDPSC-apoVs activate EC autophagy and promote EC angiogenesis via the TFEB-induced autophagy-lysosome pathway

(A) Western blotting analysis shows the presence of TUFM in apoVs derived from hDPSCs, si-NC-treated hDPSCs, and si-*TUFM*-treated hDPSCs. (B) Western blot analysis shows autophagy-associated gene (ATG7, Beclin-1, and LC3) expressions in ECs after incubation with apoVs or si-*TUFM*-apoVs. The angiogenic capacity of ECs, including tube formation (C), migration (D), and proliferation (E) were detected after treatment with apoVs or si-*TUFM*-apoVs. Scale bar, 100 μm. (F) Representative confocal

(legend continued on next page)

Revascularization of ischemic-hypoxic tissues remains an unmet need in clinical treatment. Angiogenesis causes vessel sprouting from pre-existing vessels. Attracted by proangiogenic signals, ECs migrate to form blood vessels.[31] As the angiogenic effect of apoVs was confirmed, cell apoptosis and apoV release appeared to be involved in a self-regulatory process of the aggregated hDPSCs that improved the ischemic-hypoxic environment in the root canal. Our results may explain the relationship between a certain degree of donor cell apoptosis and the beneficial efficiency of apoptosis in tissue regeneration. Our findings revealed the underlying mechanisms of stem-cell-mediated tissue regeneration and provided a reference for studying early angiogenesis in the process of donor cell integration into host tissue.

Pulpitis and pulp necrosis are common oral diseases,[32] and the most traditional treatment is root canal therapy, in which the inflamed pulp is removed and replaced with inorganic material, which results in a nonvital tooth.[33] The devitalized tooth loses nutritional supplementation to the dental hard tissue, sensitive responsiveness to hot/cold stimulation, and the ability to defend against secondary infections.[34] The aggregated hDPSC implantation has been verified to be efficacious in achieving dental pulp regeneration of immature teeth whose apical foramen is not fully developed, because blood recovery and re-infusion derived from host periapical tissues is relatively effective.[20] However, for permanent teeth, in which the apical foramen has developed, revascularization between the intracanal implants and the surrounding recipient tissue needs to be established as soon as possible to ensure hDPSC survival and differentiation.[21] In animal models, we found that hDPSC-apoVs caused host-cell infiltration into the root canal to reconstruct blood supply systems and pulp tissues feasibly, which may be a viable treatment strategy for dental pulp regeneration combined with stem cell application. Furthermore, it was interesting to find *de novo* dentin-like tissue in the tooth scaffolds of the athymic nude mouse models, because it suggested that apoVs may induce dental-pulp endogenous regeneration, but the potential biological mechanisms need further exploration.

Overall, our study provides insight into the significance of apoptosis for pulp revascularization and tissue regeneration in an ischemic-hypoxic microenvironment and elucidates the mechanistic principles underlying how hDPSC-apoVs regulate the angiogenesis of recipient ECs. Our findings provide a promising approach to restore lost pulp tissue based on hDPSC-apoVs ameliorating early revascularization and lay the foundation for roles played by EVs in organ repair and regeneration.

MATERIALS AND METHODS

Isolation, culture, and characterization of the hDPSCs

The use of dental pulp from human deciduous teeth was approved by the Ethics Committee of the Fourth Military Medical University, and informed consent was obtained from the donors. hDPSCs were isolated and cultured from the deciduous teeth using the collagenase digestion method, as previously reported.[35] When the primary hDPSCs proliferated to 80%–90% confluence, the adherent cells were digested with 0.25% trypsin (MP Biomedicals, USA) and passaged *in vitro*. Third- and fourth-generation hDPSCs were used for the experiments.

The hDPSCs were identified according to a previously reported method.[36] For the flow cytometry analysis of surface markers, hDPSCs were incubated with PE-conjugated anti-CD90 (12-0909-41, eBioscience, USA; 1:20), PE-conjugated anti-CD105 (800504, BioLegend, USA; 1:20), FITC-conjugated anti-CD73 (344015, BioLegend; 1:20), PE-conjugated anti-CD45 (304008, BioLegend; 1:20), PE-conjugated anti-CD34 (343506, BioLegend; 1:20), APC-conjugated anti-CD19 (302212, BioLegend; 1:20), FITC-conjugated anti-CD14 (325603, BioLegend; 1:20), and FITC-conjugated anti-HLA-DR (11-9956, eBioscience; 1:20) antibodies at 4°C for 30 min. The percentages of positively stained cells were analyzed with a CytoFLEX flow cytometer (Beckman Coulter, USA) and FlowJo 10.0 software (Flow Jo LLC, USA).

For colony formation, second-passage hDPSCs were collected, and 1×10^3 cells were seeded in 10-cm culture dishes. After 10 days, the cells were stained with 0.1% crystalline violet (Sigma-Aldrich, USA), and the number of colonies was calculated. For osteogenic differentiation, hDPSCs were cultured with osteogenic culture medium containing 10 mM β-glycerophosphate, 50 μg/mL ascorbic acid, and 10 nM dexamethasone (all from Sigma-Aldrich). ALP staining or alizarin red S (Sigma-Aldrich) staining were performed on day 14 or day 21, respectively. For adipogenic differentiation, hDPSCs were cultured in lipogenic medium containing 0.5 mM isobutylmethylxanthine, 1 μM dexamethasone, 10 μM insulin, and 0.2 mM indomethacin (all from Sigma-Aldrich) for 14 days and then stained with ORO (Sigma-Aldrich). Photographs were taken with an inverted optical microscope (Olympus, Japan).

Apoptosis inhibition

When the cells had proliferated to 80%–90% confluence, the medium was supplemented with 50 μM Z-VAD(ONE)-FMK (HY-16658, MCE, China). One hour later, the cells were treated with 0.5 μM

microscopy images show the number of lysosomes in ECs after treatment with apoVs or Torin 1. Scale bar, 50 μm. (G) Western blot analysis shows lysosome-associated gene (LAMP1 and CLCN7) and TFEB expressions in ECs after incubation with apoVs at concentrations of 10, 20, or 30 μg/mL. (H) Expression of TFEB in cytosolic (Cyt.) and nuclear (Nuc.) fractions was detected by western blots after treatment with apoVs or Torin 1. (I) Representative confocal microscopy images show the locations of TFEB in ECs after treatment with apoVs or Torin1. Scale bar, 25 μm. (J) Western blot analysis shows autophagy-associated gene (ATG7, Beclin-1, and LC3) expressions in ECs after decreased expression of TFEB. (K) Western blot analysis shows autophagy-associated gene (ATG7, Beclin-1, and LC3) expressions in ECs after increased expression of TFEB. After transfection with si-*TFEB*, the angiogenic capacity of ECs, including tube formation (L), migration (M), and proliferation (N) were detected following coculture with apoVs (20 μg/mL). Scale bar, 100 μm; n = 3-5 per group. Data are presented as mean ± SD. Statistical analyses were performed by Student's t test (two-tailed) for two-group comparisons and one-way ANOVA with Tukey's post hoc test or Welch's ANOVA with Games-Howell post hoc test for multiple-group comparisons. *$p < 0.05$, **$p < 0.01$, ***$p < 0.001$; ns, $p > 0.05$.

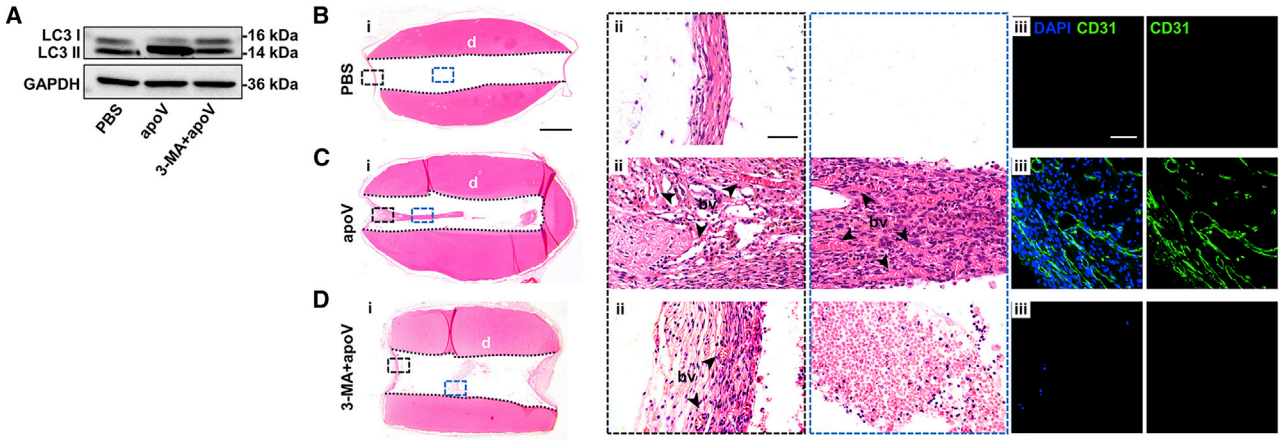

Figure 7. Autophagy is required for apoV-mediated angiogenesis in athymic nude mice model

(A) The expressions of LC3 in PBS group, apoV group, and 3-MA + apoV group were evaluated by western blots. (Bi–Di) Representative microscope images of H&E staining show regeneration of dental-pulp-like tissue in tooth scaffolds. Scale bars, 1 mm. (Bii–Dii) Enlarged view of boxed area in (i). Scale bars, 100 μm. (Biii–Diii) Immunofluorescence analysis shows the expression of blood vessel marker CD31, with positive represented by green stains. Scale bars, 50 μm; bv, blood vessels; d, dentin.

staurosporine (9953s, Cell Signaling Technology, USA) for 12 h to induce apoptosis and then stained with a TUNEL assay kit (C1088, Beyotime Biotechnology, China). The inhibitory efficiency was determined by confocal microscopy (Nikon, Japan).

Culture of aggregated hDPSCs

hDPSCs were seeded into six-well plates with 2×10^5 cells per well and cultured with α-MEM for 3 days. When the cells had reached 90% confluence, the medium was exchanged with α-MEM containing 100 mg/mL vitamin C (Invitrogen, USA) and 10% fetal bovine serum (FBS), and the culture was continued for another 10 days. The medium was changed every 2 days. When white membrane-like structures were observed, the cell aggregates were separated from the culture plates with a cell scraper.

Animal models

Animal experiments were performed in accordance with the guidelines of the Institutional Animal Care Use Committee of the Fourth Military Medical University and the ARRIVE guidelines.

Six-week-old athymic nude mice (purchased from Hunan SJA Laboratory Animal Co., Ltd.) were procured and housed under specific-pathogen-free conditions (24°C, 12-h:12-h light-dark cycle, and 50% humidity) with free access to food and water. Briefly, we prepared tooth scaffolds according to a previously reported method.[36] The mice were first allocated to four groups: the hDPSC group (aggregated hDPSCs), Z-VAD group (aggregated hDPSCs pretreated with Z-VAD), hDPSC + apoV group (aggregated hDPSC + apoVs), and Z-VAD + apoV group (aggregated hDPSC pretreated with Z-VAD + apoVs). After the aggregates were filled into the tooth scaffolds, the tooth scaffolds were buried in the dorsum of athymic nude mice under general anesthesia, with two tooth scaffolds implanted per mouse. To further explore the function of the apoVs, the mice were assigned to three groups: the PBS group (PBS), apoV group (apoVs), and 3-MA + apoV group (athymic nude mice pretreated with 3-MA + apoVs). The mice were euthanized 8 weeks after implantation, and the tooth scaffolds were collected and fixed with 4% paraformaldehyde (PFA) for follow-up histological analysis.

In addition, we established an orthotopic model with male beagle dogs (purchased from Chengdu DOSSY Experimental Animals Co., Ltd.) by removing the dental pulp. The dogs were assigned to four groups: the PBS group (treated with PBS), apoV group (treated with apoVs), Revas group (with revascularization treatment), and normal group (normal). Preoperatively, bimaxillary CBCT was performed on each beagle, and intraoperatively, gel material was injected into the root canal of the anterior tooth after removal of the pulp. After 3 months, the beagles underwent bimaxillary CBCT, and then, the anterior teeth were extracted and fixed in 4% PFA for 24 h at 4°C, followed by demineralization in 17% EDTA (pH 7.4) for 8 weeks. The tissues were subjected to a histological analysis.

Apoptosis analysis of the hDPSCs after implantation

A TUNEL staining kit (C1088, Beyotime Biotechnology) was used to detect the apoptosis ratio of the aggregated hDPSCs after implantation. Briefly, aggregated hDPSCs were removed 24, 48, or 72 h after implantation. Samples were initially frozen. The sections (10 μm thick) were later prepared by sequential pretreatment and then stained with TUNEL at 37°C for 1.5 h. Cell nuclei were stained with Hoechst 33342 (Sigma-Aldrich). Digital photographs were taken using a laser-scanning confocal microscope (Nikon) at high magnification.

In addition, aggregated cells were removed 24, 48, 72, or 96 h after implantation, digested to generate single-cell suspensions, and stained using an Annexin V/7-AAD assay kit (559763, BD Biosciences, USA) according to the manufacturer's instructions. The percentage

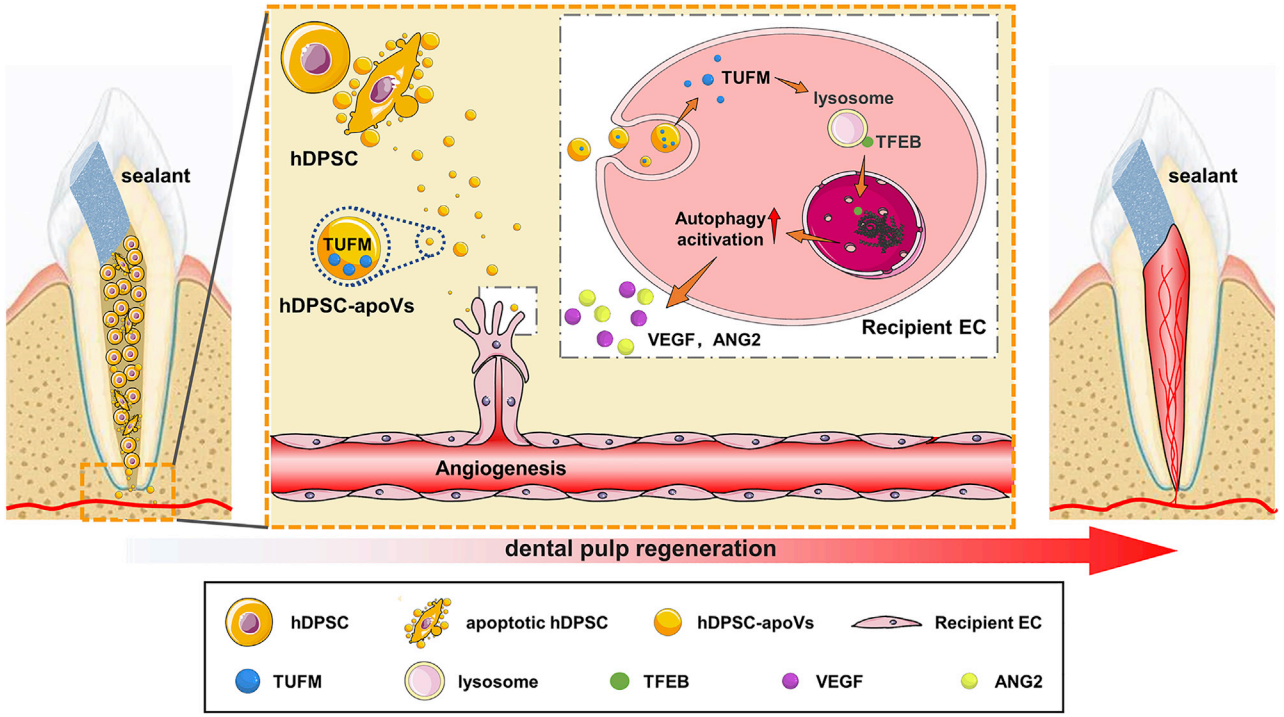

Figure 8. Schematic diagram showing the synopsis of the findings

The apoVs released from hDPSCs was able to promote EC autophagy via transferring TUFM. Furthermore, autophagy signaling activated the angiogenesis potential of ECs. Eventually, the accelerated revascularization promoted the efficient regeneration of dental pulp.

of apoptotic cells was analyzed using a CytoFLEX flow cytometer (Beckman Coulter) and FlowJo 10.0 software.

Histological and immunofluorescence analysis

Tooth samples from the aforementioned animal experiments were collected and fixed in 4% PFA and embedded in paraffin for 24 h. Serial sections (5 μm thick) of the paraffin-embedded blocks were cut and subjected to H&E staining and Masson's trichrome staining. Immunofluorescence staining was performed using standard procedures. The sections were incubated with the following antibodies: anti-CD31 (ab28364, Abcam; 1:250), anti-DSPP (sc-73632, Santa Cruz Biotechnology; 1:200), and anti-DMP1 (ab103203, Abcam; 1:100). IgG (Abcam) was used as the negative control. The secondary antibodies FITC-AffiniPure goat anti-rabbit IgG (H+L) (33107ES60, Yeasen Biotechnology, 1:100), Cy3-AffiniPure goat anti-rabbit IgG (H+L) (33108ES60, Yeasen Biotechnology, 1:100), and Alexa Fluor 488 AffiniPure goat anti-mouse IgG (H+L) (Yeasen Biotechnology, 1:100) were applied to the sections and incubated for 60 min. The samples were sealed with Antifade mounting medium with DAPI (P0131, Beyotime Biotechnology). The stained sections were viewed with a laser-scanning confocal microscope (Nikon).

Extraction and characterization of the hDPSC-apoVs

hDPSC-apoVs were isolated from culture supernatants. First, the hDPSCs were treated with 0.5 μM staurosporine (9953s, Cell Signaling Technology) for 12 h to induce apoptosis. Then, supernatants were obtained after centrifugation at 800 g for 10 min to remove the cell debris. After centrifugation at 16,000 × *g* for 30 min at 4°C, the precipitate was collected and washed twice with PBS. The morphology of the apoVs was observed by scanning electron microscopy (SEM) (Thermo Fisher, USA). The size of the apoVs was determined using dynamic light scattering. The apoVs were stained with annexin V, and the expression of anti-cleaved caspase-3 (ab32042, Abcam, 1:1,000) was detected by western blotting.

hDPSC-apoVs uptake by ECs *in vitro*

To detect the uptake of hDPSC-apoVs by human umbilical vein ECs *in vitro*, apoVs were prestained with PKH26 (Sigma-Aldrich) according to the manufacturer's instructions and added to the culture medium containing ECs. After incubation at 37°C with 5% CO_2 for 12 h, the cells were washed with PBS and fixed with 4% PFA for 30 min. Then, the cytoskeleton was stained with phalloidin-FITC (C1033, Beyotime Biotechnology), and the nuclei were stained with Hoechst 33342 (Sigma-Aldrich). Fluorescent images were taken with a laser-scanning confocal microscope (Nikon) and analyzed with ImageJ software (National Institutes of Health, USA).

Matrigel assay

Matrigel matrix substrate gel (Corning, USA) was added to 96-well plates, which were then placed in a 37°C incubator for 30 min to solidify the gel. ECs were seeded at a density of 1.5×10^4 cells per well and incubated in serum-free medium with different doses of

hDPSC-apoVs (0, 10, 20, or 30 μg/mL). After 4 h, tube formation was recorded using an inverted microscope (Olympus, Japan). The tube formation structure in five randomly selected fields of view in each well was analyzed with ImageJ software.

Cell proliferation assay

The proliferation rate of the ECs was measured by detecting MKI67/Ki67 (ab15580, Abcam, 1:200). A total of 1×10^4 ECs were seeded in confocal plates and cultured with α-MEM containing 1% FBS. After the cells had completely adhered to the well wall, different doses of hDPSC-apoVs (0, 10, 20, or 30 μg/mL) were added and then incubated for 12 h. Fluorescence imaging was performed with a laser-scanning confocal microscope (Nikon, Japan), and the proportion of positive cells in five randomly selected fields of view in each plate was determined with ImageJ software.

Transwell assay

Cell migration was quantitated using Transwell inserts with 8-μm pores (MCEP24H48, Corning). After 12 h of starvation, a total of 2×10^4 ECs in 200 μl of DMEM were plated in the Transwell insert, and medium with different doses of hDPSC-apoVs (0, 10, 20 or 30 μg/mL) was added to the lower Transwell chamber. After coculture for 5 h, unmigrated ECs were removed, and migrated ECs were washed with PBS, fixed with 4% PFA, stained with 1% crystal violet, photographed with an inverted microscope (Olympus), and counted with ImageJ software.

Proteomic analysis

Protein lysates of the hDPSCs and hDPSC-apoVs were prepared. The peptide mixture was redissolved in a 20 mM ammonium formate solution and analyzed by LC-MS/MS on an Orbitrap Fusion Lumos mass spectrometer (Thermo Fisher Scientific, USA). Tandem mass spectra were processed with PEAKS Studio version X^+ (Bioinformatics Solutions Inc., Waterloo, Canada). Finally, 1,102 differentially expressed proteins were identified. On the basis of the Gene Ontology (GO) and Kyoto Encyclopedia of Genes and Genomes (KEGG) databases, we performed functional analyses of the proteins significantly upregulated in the apoVs.

Autophagy flux assay

ECs were infected with stubRFP-sensGFP-LC3 lentivirus (GPL2001A, GENECHEM, China) for 72 h and then treated with apoVs for 0, 4, or 24 h. CQ (HY-17589A, MCE, China) was used to block the fusion of autophagosomes and lysosomes. Images were obtained with a laser-scanning confocal microscope (Nikon) and quantified with ImageJ software.

LysoTracker red staining

Each confocal plate was inoculated with 1×10^4 ECs. After the cells had completely adhered, they were cultured with fresh medium containing LysoTracker Red DND-99 (40739ES50, Yeasen) for 30 min, and then, the medium was replaced to medium containing hDPSC-apoVs, CQ (negative control; HY-17589A, MCE) or torin 1 (positive control; HY-13003, MCE), in three replicates of each group. Fluorescent images were captured with a laser-scanning confocal microscope (Nikon), and the proportion of positive cells was quantified in five random fields per well with ImageJ software.

TFEB overexpression

ECs were seeded at a density of 2×10^5 cells per well in six-well plates. After 24 h, the cells were transfected with a TFEB plasmid (P18466, Miaolingbio, China). The transfection efficiency was detected by western blot after 72 h.

siRNA knockdown

hDPSCs were transfected with a siRNA negative control (si-NC) and siRNA-*TUFM* (si-*TUFM*, GENECHEM) using the transfection reagent HitransG P (REVG005, GENECHEM) according to the manufacturer's instructions. The ECs were also transfected with siRNA negative control (si-NC) and siRNA-*TFEB* (si-*TFEB*, RiboBio, China) using a transfection kit (C10511-1, RiboBio) according to the manufacturer's instructions. The transfection efficiency was measured by western blotting after 72 h.

Protein isolation and western blotting

Total proteins of cells and tissues were extracted using RIPA buffer with added protease inhibitors. Nuclear and cytoplasmic proteins were extracted with a nuclear and cytoplasmic protein extraction kit (20126ES50, Yeasen) according to the manufacturer's instructions. Protein concentrations were assayed with BCA protein assay reagent (Beyotime Biotechnology). Equal amounts of protein samples were loaded onto SDS-PAGE gels, separated by electrophoresis and later transferred to PVDF membranes (Millipore, Germany). The membrane was blocked with 5% BSA for 2 h at room temperature and then incubated with primary antibody at 4°C overnight. After a wash with PBS containing 0.1% Tween 20 (PBST), the membranes were incubated with secondary antibodies at room temperature for 2 h. After incubation, the membranes were washed with PBST again. The blots were imaged with a Western-Light chemiluminescence detection system (Tanon, China). The following primary antibodies were used: anti-cleaved caspase-3 (ab32042, Abcam; 1:1,000), anti-GAPDH (CWBIO, CW0100; 1:5,000), anti-TUBB/beta-tubulin (CWBIO, CW0098; 1:5,000), anti-HIF-1α (36169, Cell Signaling; 1:1,000), anti-VEGF (ab46154, Abcam; 1:1,000), anti-ANG2 (ab155106, Abcam; 1:1,000), anti-MMP2 (ab92536, Abcam; 1:1,000), anti-Beclin-1 (3738, Cell Signaling Technology; 1:1,000), anti-LC3 (3868, Cell Signaling Technology; 1:1,000), anti-ATG7 (8558, Cell Signaling Technology; 1:1,000), anti-TUFM (ab173300, Abcam; 1:1,000), anti-LAMP1 (ab24170, Abcam; 1:1,000), anti-CLCN7 (DF3932, Affinity Biosciences; 1:1,000), anti-TFEB (4240, Cell Signaling Technology; 1:1,000), and anti-H3 (9715, Cell Signaling Technology; 1:1,000).

Statistical analysis

All the data are presented as means ± SD. Statistical and graph analyses were performed with SPSS software (version 25.0). For two-group comparisons, significance was assessed by Student's t test (two-tailed) or Student's t test with Welch correction (two-tailed). For multiple-group comparisons, significance was assessed

by one-way ANOVA with Tukey's post hoc test or Welch's ANOVA with Games-Howell post hoc test. Values of $p < 0.05$ were considered statistically significant.

SUPPLEMENTAL INFORMATION

Supplemental information can be found online at https://doi.org/10.1016/j.ymthe.2022.05.006.

ACKNOWLEDGMENTS

This work was supported by the National Key Research and Development Program of China (2021YFA1100600 to K.X.), National Natural Science Foundation of China (82071075 to K.X., 31800817 to Siying Liu, 31870970 to J.Z.), the Innovative Talent Project of Shaanxi province (2020KJXX-057 to Shiyu Liu), the Science Research Cultivation Program of Stomatological Hospital, Southern Medical University (PY2021010 to X.Y.), and the open project of State Key Laboratory of Military Stomatology (Grant No. 2020KA01 to Shiyu Liu).

AUTHOR CONTRIBUTIONS

Z.L., M.W., and Siying Liu contributed equally to the experimental performing, data acquisition and analysis, and manuscript drafting; X.L., Y.H., and Q.Y. contributed to animal experiments; Xiaoxue Yang, H.G., and A.L. contributed to data analysis and interpretation; X.H., Xiaoshan Yang, and F.D. contributed to flow cytometry analysis; H.X., J.Z., and P.L. contributed to data interpretation; Shiyu Liu, Y.J., and K.X. contributed to the study conception and design, data interpretation, and manuscript revision. All authors read and approved the final version of the manuscript.

DECLARATION OF INTERESTS

The authors declare no competing interests.

REFERENCES

1. Eelen, G., Treps, L., Li, X., and Carmeliet, P. (2020). Basic and Therapeutic Aspects of Angiogenesis Updated. Circ. Res. *127*, 310–329. https://doi.org/10.1161/CIRCRESAHA.120.316851.
2. Carmeliet, P., and Jain, R.K. (2011). Molecular mechanisms and clinical applications of angiogenesis. Nature *473*, 298–307. https://doi.org/10.1038/nature10144.
3. Aghazadeh, Y., Khan, S.T., Nkennor, B., and Nunes, S.S. (2022). Cell-based therapies for vascular regeneration: Past, present and future. Pharmacol. Ther *231*, 107976. https://doi.org/10.1016/j.pharmthera.2021.107976.
4. Schwartz, M.A., Vestweber, D., and Simons, M.J.S. (2018). A unifying concept in vascular health and disease. Science *360*, 270–271. https://doi.org/10.1126/science.aat3470.
5. Yancopoulos, G., Davis, S., Gale, N.W., Gale, N., Rudge, J.S., Rudge, J., Wiegand, S.J., Wiegand, S., and Holash, J.J.N. (2000). Vascular-specific growth factors and blood vessel formation. Nature *407*, 242–248. https://doi.org/10.1038/35025215.
6. Bronckaers, A., Hilkens, P., Martens, W., Gervois, P., Ratajczak, J., Struys, T., and Lambrichts, I. (2014). Mesenchymal stem/stromal cells as a pharmacological and therapeutic approach to accelerate angiogenesis. Pharmacol. Ther. *143*, 181–196. https://doi.org/10.1016/j.pharmthera.2014.02.013.
7. Hung, S.C., Pochampally, R.R., Chen, S.C., Hsu, S.C., and Prockop, D.J.S.c. (2007). Angiogenic Effects of Human Multipotent Stromal Cell Conditioned Medium Activate the PI3K-Akt Pathway in Hypoxic Endothelial Cells to Inhibit Apoptosis, Increase Survival, and Stimulate Angiogenesis, increase survival, and stimulate angiogenesis. Stem Cells *25*, 2363–2370. https://doi.org/10.1634/stemcells.2006-0686.
8. Yu, M., Liu, W., Li, J., Lu, J., Lu, H., Jia, W., and Liu, F. (2020). Exosomes derived from atorvastatin-pretreated MSC accelerate diabetic wound repair by enhancing angiogenesis via AKT/eNOS pathway. Stem Cell Res. Ther. *11*, 350. https://doi.org/10.1186/s13287-020-01824-2.
9. Au, P., Tam, J., Fukumura, D., and Jain, R.K. (2008). Bone marrow-derived mesenchymal stem cells facilitate engineering of long-lasting functional vasculature. Blood *111*, 4551–4558. https://doi.org/10.1182/blood-2007-10-118273.
10. Leszczynska, K.B., Foskolou, I.P., Abraham, A.G., Anbalagan, S., Tellier, C., Haider, S., Span, P.N., O'Neill, E.E., Buffa, F.M., and Hammond, E.M. (2015). Hypoxia-induced p53 modulates both apoptosis and radiosensitivity via AKT. J. Clin. Invest. *125*, 2385–2398. https://doi.org/10.1172/jci80402.
11. György, B., Szabó, T.G., Pásztói, M., Pál, Z., Misják, P., Aradi, B., László, V., Pállinger, E., Pap, E., Kittel, A., et al. (2011). Membrane vesicles, current state-of-the-art: emerging role of extracellular vesicles. Cell. Mol. Life Sci. *68*, 2667–2688. https://doi.org/10.1007/s00018-011-0689-3.
12. Liu, D., Kou, X., Chen, C., Liu, S., Liu, Y., Yu, W., Yu, T., Yang, R., Wang, R., Zhou, Y., and Shi, S. (2018). Circulating apoptotic bodies maintain mesenchymal stem cell homeostasis and ameliorate osteopenia via transferring multiple cellular factors. Cell Res. *28*, 918–933. https://doi.org/10.1038/s41422-018-0070-2.
13. Chera, S., Ghila, L., Dobretz, K., Wenger, Y., Bauer, C., Buzgariu, W., Martinou, J.C., and Galliot, B. (2009). Apoptotic cells provide an unexpected source of Wnt3 signaling to drive hydra head regeneration. Dev. Cell *17*, 279–289. https://doi.org/10.1016/j.devcel.2009.07.014.
14. Medina, C.B., Mehrotra, P., Arandjelovic, S., Perry, J.S.A., Guo, Y., Morioka, S., Barron, B., Walk, S.F., Ghesquiere, B., Krupnick, A.S., et al. (2020). Metabolites released from apoptotic cells act as tissue messengers. Nature *580*, 130–135. https://doi.org/10.1038/s41586-020-2121-3.
15. Kroemer, G., and Pietrocola, F. (2020). The scent of death: a metabolic goodbye signal emitted by dying cells. Cell Death Differ. *27*, 2030–2032. https://doi.org/10.1038/s41418-020-0533-0.
16. Todorova, D., Simoncini, S., Lacroix, R., Sabatier, F., and Dignat-George, F. (2017). Extracellular Vesicles in Angiogenesis. Circ. Res. *120*, 1658–1673. https://doi.org/10.1161/CIRCRESAHA.117.309681.
17. EL Andaloussi, S., Mager, I., Breakefield, X.O., and Wood, M.J.A. (2013). Extracellular vesicles: biology and emerging therapeutic opportunities. Nat. Rev. Drug Discov. *12*, 347–357. https://doi.org/10.1038/nrd3978.
18. Ivanovski, S., Vaquette, C., Gronthos, S., Hutmacher, D., and Bartold, P.M. (2014). Multiphasic scaffolds for periodontal tissue engineering. J. Dent. Res. *93*, 1212–1221. https://doi.org/10.1177/0022034514544301.
19. Xu, H., Wang, P., Wang, L., Bao, C., Chen, Q., Weir, M., Chow, L., Zhao, L., Zhou, X., and Reynolds, M.J. (2017). Calcium phosphate cements for bone engineering and their biological properties. Bone Res. *5*, 17056. https://doi.org/10.1038/boneres.2017.56.
20. Xuan, K., Li, B., Guo, H., Sun, W., Kou, X., He, X., Zhang, Y., Sun, J., Liu, A., Liao, L., et al. (2018). Deciduous autologous tooth stem cells regenerate dental pulp after implantation into injured teeth. Sci. Transl. Med. *10*. https://doi.org/10.1126/scitranslmed.aaf3227.
21. Rombouts, C., Giraud, T., Jeanneau, C., and About, I. (2017). Pulp Vascularization during Tooth Development, Regeneration, and Therapy. J. Dent. Res. *96*, 137–144. https://doi.org/10.1177/0022034516671688.
22. Sui, B., Chen, C., Kou, X., Li, B., Xuan, K., Shi, S., and Jin, Y. (2019). Pulp Stem Cell-Mediated Functional Pulp Regeneration. J. Dent. Res. *98*, 27–35. https://doi.org/10.1177/0022034518808754.
23. Filipowska, J., Tomaszewski, K.A., Niedzwiedzki, L., Walocha, J.A., and Niedzwiedzki, T. (2017). The role of vasculature in bone development, regeneration and proper systemic functioning. Angiogenesis *20*, 291–302. https://doi.org/10.1007/s10456-017-9541-1.
24. Fernandez, A., Ordonez, R., Reiter, R.J., Gonzalez-Gallego, J., and Mauriz, J.L. (2015). Melatonin and endoplasmic reticulum stress: relation to autophagy and apoptosis. J. Pineal Res. *59*, 292–307. https://doi.org/10.1111/jpi.12264.
25. Chandra, A., Rick, J., Yagnik, G., and Aghi, M.K. (2020). Autophagy as a mechanism for anti-angiogenic therapy resistance. Semin. Cancer Biol. *66*, 75–88. https://doi.org/10.1016/j.semcancer.2019.08.031.

26. Kim, D., Hwang, H.Y., and Kwon, H.J. (2021). A natural small molecule induces MAPT clearance via mTOR-independent autophagy. Biochem. Biophys. Res. Commun. *568*, 30–36. https://doi.org/10.1016/j.bbrc.2021.06.060.

27. Medina, D.L., Di Paola, S., Peluso, I., Armani, A., De Stefani, D., Venditti, R., Montefusco, S., Scotto-Rosato, A., Prezioso, C., Forrester, A., et al. (2015). Lysosomal calcium signalling regulates autophagy through calcineurin and TFEB. Nat. Cell Biol. *17*, 288–299. https://doi.org/10.1038/ncb3114.

28. Russell, L.D., Chiarini-Garcia, H., Korsmeyer, S.J., and Knudson, C.M. (2002). Bax-Dependent Spermatogonia Apoptosis Is Required for Testicular Development and Spermatogenesis1. Biol. Reprod. *66*, 950–958. https://doi.org/10.1095/biolreprod66.4.950.

29. Hafezi, F., Marti, A., Munz, K., and REMÉ, C.E. (1997). Light-induced apoptosis: differential timing in the retina and pigment epithelium. Exp. Eye Res. *64*, 963–970. https://doi.org/10.1006/exer.1997.0288.

30. Lu, L., and Osmond, D.G. (2000). Apoptosis and its modulation during B lymphopoiesis in mouse bone marrow. Immunol. Rev. *175*, 158–174. https://doi.org/10.1111/j.1600-065x.2000.imr017506.x.

31. Potente, M., Gerhardt, H., and Carmeliet, P. (2011). Basic and therapeutic aspects of angiogenesis. Cell *146*, 873–887. https://doi.org/10.1016/j.cell.2011.08.039.

32. Chen, H., Fu, H., Wu, X., Duan, Y., Zhang, S., Hu, H., Liao, Y., Wang, T., Yang, Y., Chen, G., et al. (2020). Regeneration of pulpo-dentinal–like complex by a group of unique multipotent CD24a $^{+}$ stem cells. Sci. Adv. *6*, eaay1514. https://doi.org/10.1126/sciadv.aay1514.

33. journal, J.I. (2006). Quality guidelines for endodontic treatment: consensus report of the European Society of Endodontology. Eur. Soc. Endodontol. *39*, 921–930. https://doi.org/10.1111/j.1365-2591.2006.01180.x.

34. Gong, T., Heng, B.C., Lo, E.C.M., and Zhang, C. (2016). Current Advance and Future Prospects of Tissue Engineering Approach to Dentin/Pulp Regenerative Therapy. Stem Cells Int. *2016*, 1–13. https://doi.org/10.1155/2016/9204574.

35. Miura, M., Gronthos, S., Zhao, M., Lu, B., Fisher, L.W., Robey, P.G., and Shi, S.J. (2003). SHED: stem cells from human exfoliated deciduous teeth. Proc. Natl. Acad. Sci. U S A *100*, 5807–5812. https://doi.org/10.1073/pnas.0937635100.

36. Wu, M., Liu, X., Li, Z., Huang, X., Guo, H., Guo, X., Yang, X., Li, B., Xuan, K., and Jin, Y. (2021). SHED aggregate exosomes shuttled miR-26a promote angiogenesis in pulp regeneration via TGF-β/SMAD2/3 signalling. Cell Prolif. *54*, e13074. https://doi.org/10.1111/cpr.13074.

YMTHE, Volume *30*

Supplemental Information

Apoptotic vesicles activate autophagy in recipient cells to induce angiogenesis and dental pulp regeneration

Zihan Li, Meiling Wu, Siying Liu, Xuemei Liu, Yu Huan, Qingyuan Ye, Xiaoxue Yang, Hao Guo, Anqi Liu, Xiaoyao Huang, Xiaoshan Yang, Feng Ding, Haokun Xu, Jun Zhou, Peisheng Liu, Shiyu Liu, Yan Jin, and Kun Xuan

Supplementary Figures

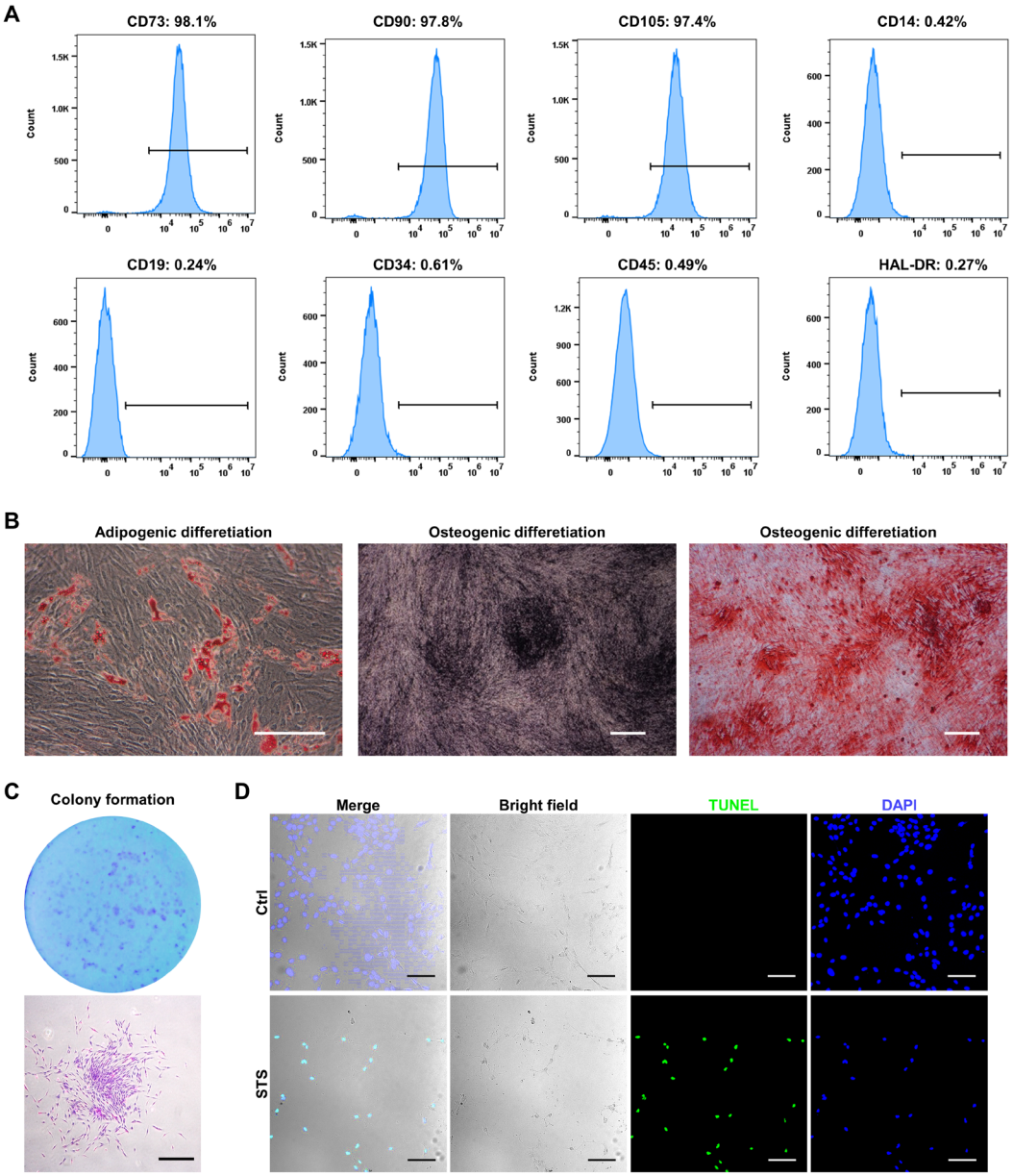

Figure S1. Characterization of human deciduous pulp stem cell (hDPSC).

(A) Flow cytometric analysis revealed positive expression of CD73, CD90, CD105, and negative expression of CD13, CD19, CD34, CD45 and HAL-DR. **(B)** Oil red O staining, alkaline phosphatase staining and Alizarin red S staining of hDPSCs after being induced in adipogenic or osteogenic medium. Scale bar, 250 μm. **(C)** Crystalline violet staining showed the colony formation ability of hDPSCs. Scale bar, 250 μm. **(D)** Representative bright field and terminal deoxynucleotidyl transferase dUTP nick end labeling (TUNEL) (green) staining images of hDPSCs and staurosporine (STS)-induced apoptotic hDPSCs, counterstained by DAPI (blue). Scale bars, 100 μm (TUNEL staining).

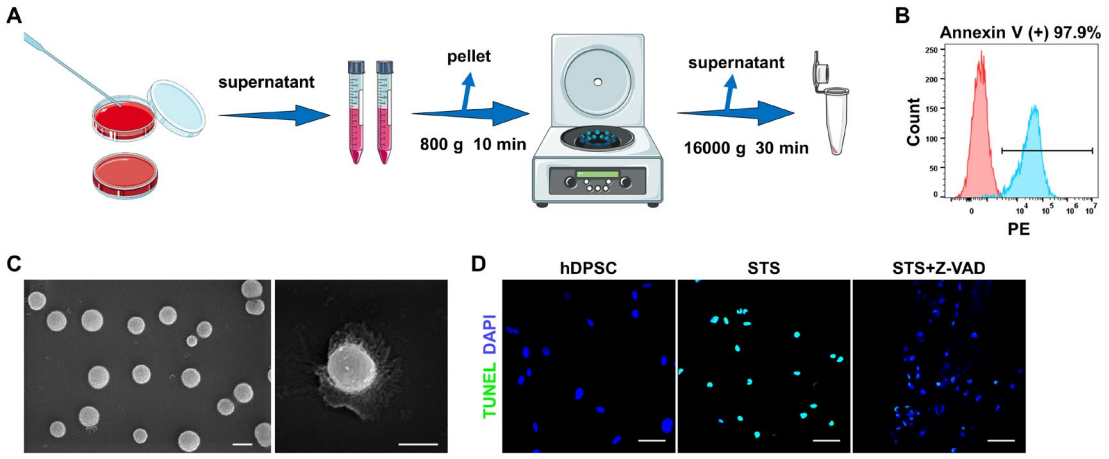

Figure S2. Isolation, identification of apoptotic vesicles derived from hDPSC (hDPSC-apoVs).

(A) Flow chart showed the protocol of isolate apoptotic extracellular vesicles from hDPSC. **(B)** Flow cytometric analysis of Annexin V staining in apoVs. **(C)** Representative wide scanning electron microscope (SEM) image showed the morphology of apoVs. Scale bar, 200 nm. **(D)** Terminal deoxynucleotidyl transferase dUTP nick end labeling (TUNEL) (green) staining images of hDPSCs pretreated with Z-VAD, counterstained by DAPI (blue). Scale bars, 50 μm. (TUNEL staining).

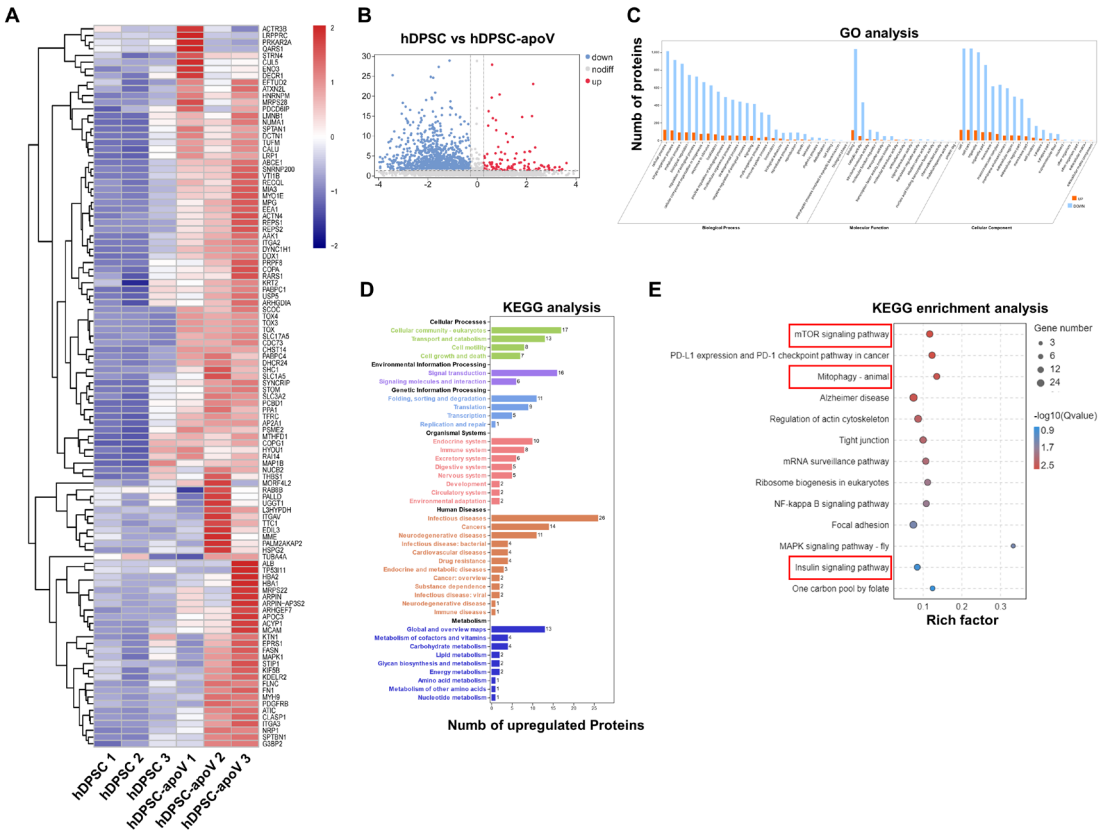

Figure S3. Proteomic analysis of hDPSC and hDPSC-apoVs.

(A) Hierarchical clustering of differentially expressed proteins (DEPs) (Fold change > 1.5 and P value < 0.05) between hDPSC and hDPSC-apoV, with protein abundance being Z-score normalized. Rows represent proteins and columns represent individual replicates. **(B)** Volcano plot showed significantly upregulated (red dots) and downregulated (blue dots) proteins in apoVs, compared to hDPSCs. **(C)** Gene ontology (GO) analysis of significantly differentially expressed proteins in apoVs, categorized into “Cellular component”, “Molecular function” and “Biological process”. **(D)** Kyoto Encyclopedia of Genes and Genomes (KEGG) pathway analysis of significantly upregulated proteins in apoVs. **(E)** KEGG pathway enrichment analysis of upregulated proteins in apoVs. The enriched KEGG pathways were presented as a bubble chart. The Y-axis represents KEGG pathways and the X-axis represents rich factor. The color of the bubble represented enrichment significance and the size of the bubble represented the number of upregulated proteins.